Can molecular simulations reliably compare homogeneous and heterogeneous ice nucleation?

Dominic Atherton, 🆔 **Angelos Michaelides and** 🆔 **Stephen J. Cox**

View Online Export Citation CrossMark

Can molecular simulations reliably compare homogeneous and heterogeneous ice nucleation?

View Online   Export Citation   CrossMark

Dominic Atherton, Angelos Michaelides, [iD] [iD] and Stephen J. Cox[a] [iD]

AFFILIATIONS

Yusuf Hamied Department of Chemistry, University of Cambridge, Lensfield Road, Cambridge CB2 1EW, United Kingdom

[a]Author to whom correspondence should be addressed: sjc236@cam.ac.uk

ABSTRACT

In principle, the answer to the posed titular question is undoubtedly "yes." But in practice, requisite reference data for homogeneous systems have been obtained with a treatment of intermolecular interactions that is different from that typically employed for heterogeneous systems. In this article, we assess the impact of the choice of truncation scheme when comparing water in homogeneous and inhomogeneous environments. Specifically, we use explicit free energy calculations and a simple mean field analysis to demonstrate that using the "cut-and-shift" version of the Lennard-Jones potential (common to most simple point charge models of water) results in a systematic increase in the melting temperature of ice I_h. In addition, by drawing an analogy between a change in cutoff and a change in pressure, we use existing literature data for homogeneous ice nucleation at negative pressures to suggest that enhancements due to heterogeneous nucleation may have been overestimated by several orders of magnitude.

I. INTRODUCTION

The formation of ice is a process of great importance across a broad range of fields from climate science[1,2] to biology.[3] Obtaining a detailed molecular-level understanding of both homogeneous nucleation (i.e., in the absence of foreign bodies such as mineral particles) and heterogeneous nucleation (i.e., in the presence of surfaces due to foreign bodies) has attracted major research efforts from both experimental and simulation groups.[4,5] With regard to the latter, in a bid to reduce computational cost, most molecular simulations employ empirical potentials that approximately describe the interactions between water molecules. While many types of empirical potentials exist,[6–8] simple point charge (SPC) models are one of the most commonly used. Note that we use "SPC model" to refer to the general class of water models detailed in Sec. I A rather than the specific water model of Ref. 9. In addition to being relatively simple and computationally efficient, an appealing feature of SPC models is that they preserve the donor–acceptor nature of water's hydrogen-bond network, which can be especially important for heterogeneous nucleation, e.g., in the presence of kaolinite.[10,11]

To ensure short-ranged repulsion between molecules, most commonly used SPC water models, at least formally, employ the Lennard-Jones (LJ) potential,[12]

$$u_{LJ}^{(\infty)}(r) = 4\varepsilon\left[\left(\frac{\sigma}{r}\right)^{12} - \left(\frac{\sigma}{r}\right)^6\right], \qquad (1)$$

which is parameterized by an energy scale ε and length scale σ, where r indicates the distance between two water molecules (usually the separation between their oxygen atoms). Figure 1(a) shows $u_{LJ}^{(\infty)}$.

In addition to explicit electrostatic interactions between water molecules, the $-(\sigma/r)^6$ term contributes to the cohesive energy of the system. Despite being the basis for most SPC water models, however, $u_{LJ}^{(\infty)}$ is rarely sampled explicitly; due to the infinite range of the attractive $-(\sigma/r)^6$ term, it is common to truncate $u_{LJ}^{(\infty)}$ in some fashion (see, e.g., Refs. 13 and 14). Two common procedures, which we detail in Sec. I A, are to use "tail corrections" or to "cut-and-shift," as shown in Figs. 1(a) and 1(b), respectively. By comparing these plots, it can be seen that, while similar, these two truncation procedures result in different intermolecular potentials and will, in general, have different properties. For example, thermodynamic properties such as interfacial tension and the location of phase boundaries are known to be affected.[15–20]

Why then would another article that investigates the effects of truncating the LJ potential be useful? Put simply, the phase behavior of SPC water models has been studied extensively using the
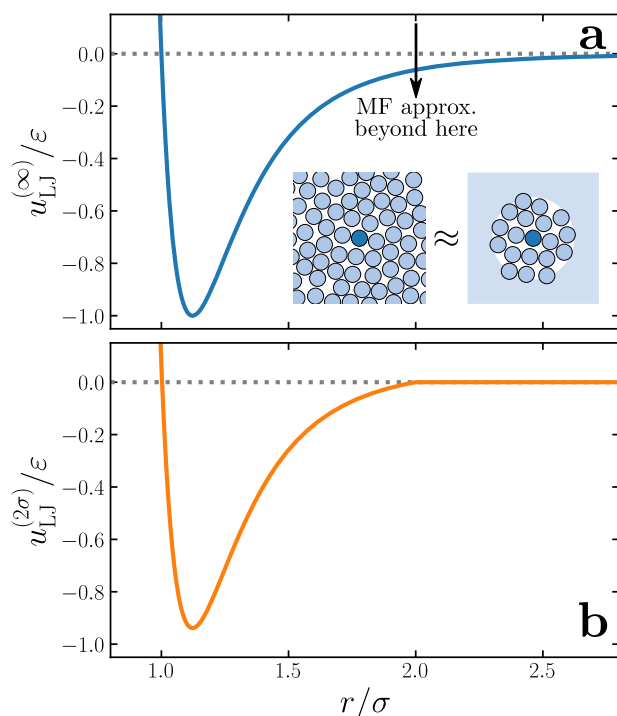
FIG. 1. The two variations of the LJ potential studied in this article. (a) The solid blue curve shows $u_{\mathrm{LJ}}^{(\infty)}$ given by Eq. (1). For *homogeneous* systems, $u_{\mathrm{LJ}}^{(\infty)}$ is well-approximated by truncating interactions at a given cutoff (indicated by the arrow) and applying "tail corrections" to account for neglected interactions; this is equivalent to a mean field approximation. Inset: schematic representation of the tail-correction procedure. The blue shaded region indicates that interactions between the tagged particle (dark blue) and those beyond the cutoff radius are accounted for in an average sense. (b) The "cut-and-shift" variant of the LJ potential [see Eq. (7)] has vanishing interactions beyond the cutoff. It is a different potential with different properties compared to $u_{\mathrm{LJ}}^{(\infty)}$. In both examples, the cutoff radius is 2σ.

tail-corrected truncation scheme.[21–24] And the same can be said for most calculations of homogeneous ice nucleation rates.[25–28] Yet, as we will discuss in more detail in the following, the use of tail corrections makes direct comparison to inhomogeneous systems challenging. While a simple approach to mitigate discrepancies between homogeneous and inhomogeneous systems would be consistent use of cut-and-shift potentials, it is unreasonable to expect that each study of heterogeneous nucleation is accompanied by (i) a full recalculation of the melting temperature or phase diagram and (ii) recomputation of the homogeneous nucleation rate. [To give a sense of perspective, in Ref. 26, over 21×10^6 central processing unit (CPU) hours were required to compute the homogeneous nucleation rate with forward flux sampling (FFS).] In this article, we address the first issue directly by outlining a procedure to approximately predict the change in melting temperature between the tail-corrected and cut-and-shift systems. We then combine our results with those in Ref. 28 to estimate the impact on the comparison of homogeneous and heterogeneous nucleation rates.

A. Formulating the problem

We now detail the tail-correction and cut-and-shift truncation schemes as well as illustrate the inconsistencies that appear between homogeneous and inhomogeneous systems. We are concerned with SPC water models that formally have a potential energy function of the kind

$$U^{(\infty)}(\mathbf{R}^N) = \sum_{i<j}^{N} u_{\mathrm{LJ}}^{(\infty)}(|\mathbf{r}_{ij}^{(\mathrm{O})}|) + \sum_{i<j}^{N}\sum_{\alpha,\beta} \frac{q^{(\alpha)}q^{(\beta)}}{|\mathbf{r}_j^{(\alpha)} - \mathbf{r}_i^{(\beta)}|}, \quad (2)$$

where $\mathbf{R}^N$ denotes the set of atomic positions for a configuration of N water molecules, $\mathbf{r}_{ij}^{(\mathrm{O})}$ is the separation vector between the oxygen atoms of molecules i and j, and $q_i^{(\alpha)}$ is the charge of site α, located at $\mathbf{r}_i^{(\alpha)}$, of molecule i. (We adopt a unit system in which $4\pi\epsilon_0 = 1$, where ϵ_0 is the permittivity of free space.) The second set of sums in Eq. (2), which we will denote U_{elec} hereafter, describes electrostatic interactions between molecules, while the first set of sums involves the LJ potential. For SPC models of water, the choice of $u_{\mathrm{LJ}}^{(\infty)}$ is rooted in grounds of convention and convenience, rather than having any deep theoretical justification. Nonetheless, SPC models of water formally described by Eq. (2) have been, are, and will likely continue (at least in the near future) to be the foundation for many molecular simulations of water's condensed phases.

So far, we have referred to SPC models of water that are "formally" described by the potential energy given in Eq. (2). But as already mentioned, in practice, $u_{\mathrm{LJ}}^{(\infty)}$ is usually truncated in some fashion.[13,14] For the tail-correction scheme, one employs a simple truncation,

$$u_{\mathrm{LJ}}^{(r_c\to\infty)}(r) = \begin{cases} u_{\mathrm{LJ}}^{(\infty)}(r), & r \le r_c, \\ 0, & r > r_c, \end{cases} \quad (3)$$

and then approximately accounts for the effects of truncation by adding a mean field (MF) correction,

$$\frac{\Delta_{\mathrm{MF}}U(r_c)}{N} = \frac{8\pi\epsilon\tilde{\rho}\sigma^3}{9}\left[\left(\frac{\sigma}{r_c}\right)^9 - 3\left(\frac{\sigma}{r_c}\right)^3\right], \quad (4)$$

to the total potential energy,

$$U^{(\infty)}(\mathbf{R}^N) \approx U^{(r_c\to\infty)}(\mathbf{R}^N)$$
$$= \sum_{i<j}^{N} u_{\mathrm{LJ}}^{(r_c\to\infty)}(|\mathbf{r}_{ij}^{(\mathrm{O})}|) + \Delta_{\mathrm{MF}}U(r_c) + U_{\mathrm{elec}}(\mathbf{R}^N), \quad (5)$$

where $\tilde{\rho}$ is the average number density. The superscript "$(r_c \to \infty)$" indicates that when used in combination with $\Delta_{\mathrm{MF}}U(r_c)$, a system that employs $u_{\mathrm{LJ}}^{(r_c\to\infty)}$ satisfies $U^{(r_c\to\infty)} \approx U^{(\infty)}$; this is reasonable provided that $g_{\mathrm{OO}}(r \ge r_c) \approx 1$, where g_{OO} is the oxygen–oxygen pair correlation function. In a similar spirit, the pressure can also be corrected in a MF fashion,

$$\Delta_{\mathrm{MF}}p(r_c) = \frac{32\pi\epsilon\tilde{\rho}^2\sigma^3}{9}\left[\left(\frac{\sigma}{r_c}\right)^9 - \frac{3}{2}\left(\frac{\sigma}{r_c}\right)^3\right]. \quad (6)$$

A comment is in order concerning the functional form of $u_{\mathrm{LJ}}^{(r_c\to\infty)}$ [Eq. (3)]. The discontinuity at r_c suggests the presence of impulsive forces. Impulsive forces, however, are challenging to implement

in molecular dynamics simulations, and it is standard practice to neglect them entirely. Moreover, as interactions beyond r_c are not neglected in $U^{(r_c \to \infty)}$ but instead accounted for in a mean field fashion, we argue (see the supplementary material) that this neglect of impulsive forces is, in fact, consistent with the use of $\Delta_{MF}U$ and $\Delta_{MF}p$ as it accounts for a pointwise cancellation of impulsive forces.

The alternative cut-and-shift truncation scheme is

$$u_{LJ}^{(r_c)}(r) = \begin{cases} u_{LJ}^{(\infty)}(r) - u_{LJ}^{(\infty)}(r_c), & r \leq r_c, \\ 0, & r > r_c, \end{cases} \tag{7}$$

such that the total potential energy is

$$U^{(r_c)}(\mathbf{R}^N) = \sum_{i<j}^{N} u_{LJ}^{(r_c)}(|\mathbf{r}_{ij}^{(O)}|) + U_{elec}(\mathbf{R}^N). \tag{8}$$

We will use the superscript "(r_c)" to indicate that $u_{LJ}^{(r_c)}$ is used. (We will, on occasion, drop the superscript notation either because it is clear from context which truncation scheme is relevant or because it is unimportant to differentiate between truncation schemes. When a numerical value of r_c is specified, it will be given in Ångstrom although we will omit units from the superscript.) For simulations of systems in the canonical (NVT) ensemble, dynamics are unaffected by the choice of $U^{(r_c)}$ vs $U^{(r_c \to \infty)}$. The pressure, however, is sensitive to the choice of truncation scheme,

$$p^{(r_c \to \infty)} \approx p^{(r_c)} + \Delta_{MF}p(r_c). \tag{9}$$

The implication of Eq. (9) is that dynamics in the isothermal–isobaric (NpT) ensemble are affected by the choice of $U^{(r_c)}$ vs $U^{(r_c \to \infty)}$. Furthermore, systems employing $U^{(r_c \to \infty)}$ and $U^{(r_c)}$ will have for the same r_c different equations of state.[15,16]

Implicit in our above discussion of MF corrections is that the system is homogeneous such that the average equilibrium density $\langle \rho(\mathbf{r}) \rangle = \bar{\rho}$ does not depend upon the position $\mathbf{r}$ in the fluid, as shown in Fig. 2(a). If the system of interest is inhomogeneous, such as liquid water in coexistence with its vapor, a typical simulation approach is to employ the NVT ensemble with a cuboidal cell that has an elongated dimension along the average surface normal; such a scenario is depicted in Fig. 2(b). As $\Delta_{MF}U$ and $\Delta_{MF}p$ do not affect dynamics in the NVT ensemble, effects of using $U^{(r_c \to \infty)}$ for inhomogeneous systems would perhaps seem benign, resulting simply in a shift of the energy, i.e., $U^{(r_c \to \infty)}(\mathbf{R}^N) - U^{(\infty)}(\mathbf{R}^N) = const.$

Potential problems arise, however, concerning thermodynamic consistency between the homogeneous and inhomogeneous systems. This is demonstrated in Fig. 3 for TIP4P/ice[24]—a commonly used SPC water model for studying ice formation—at 300 K with $r_c = 8.5$ Å. Figure 3(a) shows the average mass density $\bar{\rho}_m(p)$ obtained from simulations of the homogeneous fluid employing either TIP4P/ice$^{(8.5 \to \infty)}$ or TIP4P/ice$^{(8.5)}$. Figure 3(b) shows the equilibrium mass density profile $\langle \rho_m(z) \rangle$ for a film of TIP4P/ice$^{(8.5 \to \infty)}$ water ~40 Å thick with its liquid/vapor interface spanning the xy plane.[29] Owing to the low vapor pressure of water, $p \approx 0$ in the vapor phase. As the normal component of the pressure tensor is independent of z for a planar interface and furthermore isotropic for z in a
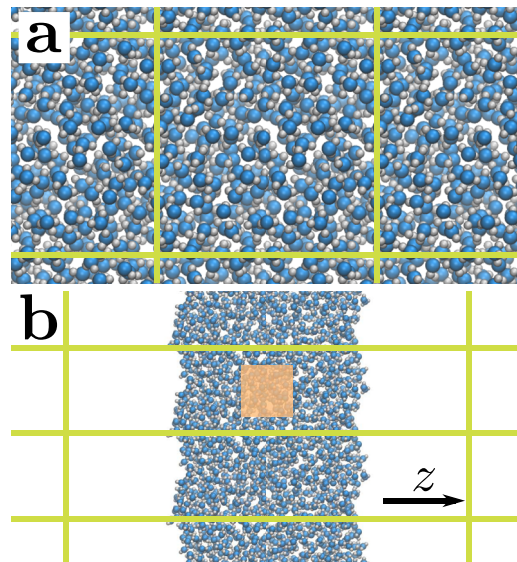

FIG. 2. Typical simulation geometries for water. (a) Homogeneous bulk water simulated under 3D bulk periodic boundary conditions such that the average density is independent of position, $\langle \rho(\mathbf{r}) \rangle = \bar{\rho}(p)$. (b) The slab geometry employed to study interfacial systems also employs periodic boundary conditions (often in 3D) and has a density profile that varies with position z along the surface normal such that, in general, $\langle \rho(z) \rangle \neq \bar{\rho}$. For thick enough slabs, regions far removed from the interfaces (as indicated, e.g., by the orange box) have an average density equal to $\bar{\rho}(p = 0)$ for the homogeneous system. Green lines indicate the boundaries of the periodically repeated simulation cells.

bulk-like fluid region, it immediately follows that $p \approx 0$ deep in the slab's interior.[30] Thermodynamic consistency then requires that

$$\frac{1}{\ell_{bulk}} \int_{\ell_{bulk}} dz \, \langle \rho_m(z) \rangle = \bar{\rho}_m(p = 0)$$

for TIP4P/ice$^{(8.5 \to \infty)}$, where ℓ_{bulk} is a length over which $\langle \rho_m(z) \rangle$ is bulk-like, as indicated, e.g., by the orange rectangles in Figs. 2(b) and 3(b). The result of such an averaging procedure is indicated by the orange-filled circle in Fig. 3(a); it is clearly inconsistent with $\bar{\rho}_m(p = 0)$ obtained from the homogeneous TIP4P/ice$^{(8.5 \to \infty)}$ simulation. As dynamics in the NVT ensemble are unaffected by the choice of $U^{(r_c)}$ vs $U^{(r_c \to \infty)}$, we might expect, and indeed observe, that the result is instead consistent with $\bar{\rho}_m(p = 0)$ for TIP4P/ice$^{(8.5)}$.

While schemes for effectively sampling $U^{(\infty)}$ do exist for heterogeneous systems (e.g., one can treat the attractive $-(\sigma/r)^6$ term in a Ewald fashion[31–34] or use mean field corrections that take the heterogeneous nature of the system into account[35–40]), their use is relatively limited compared to that of SPC water models. In addition, as discussed in Sec. I, no discrepancies would be observed with the consistent use of $U^{(r_c)}$ for both the homogeneous and inhomogeneous systems, but information concerning phase behavior and homogeneous nucleation rates relevant to $U^{(r_c)}$ systems is scarce. In Sec. II, we therefore assess the effect of using $U^{(r_c)}$ instead of $U^{(r_c \to \infty)}$ on the melting temperature T_m of ice I_h for SPC models of water. In particular, we focus on TIP4P/ice[24] and TIP4P/2005[23]
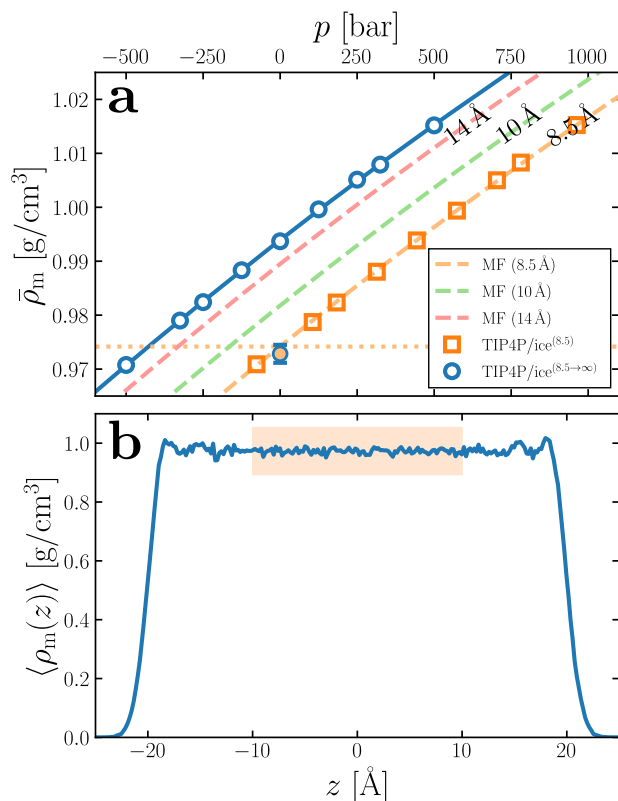
FIG. 3. Evaluating the impact of r_c on $\bar{\rho}_m$ for liquid TIP4P/ice at 300 K. (a) $\bar{\rho}_m(p)$ for a homogeneous system. White-filled circles show results from constant-p simulations of TIP4P/ice$^{(8.5\to\infty)}$, and the solid blue line indicates a quadratic fit. Dashed lines indicate MF predictions [Eq. (9), see also Sec. III] for different r_c, as indicated in the legend (the lines are also labeled). Orange squares show results from constant-p simulations of TIP4P/ice$^{(8.5)}$. The dotted line indicates $\bar{\rho}_m(p=0)$ for TIP4P/ice$^{(8.5)}$, which intercepts the TIP4P/ice$^{(8.5\to\infty)}$ results at $p \approx -427$ bars. (b) $\langle\rho_m(z)\rangle$ for a film of TIP4P/ice$^{(8.5\to\infty)}$ in contact with its vapor (only part of the simulation cell is shown). Spatially averaging $\langle\rho_m(z)\rangle$ in the slab's interior, as indicated by the shaded region, gives an estimate for $\bar{\rho}_m(0)$, which is plotted with the orange-filled circle in (a).

as these are most commonly used in simulations of ice nucleation. We stress, however, that the findings presented in this work readily extend to any SPC water model of the kind formally described by Eq. (2). To illustrate our findings, we will focus exclusively on results for TIP4P/ice in the main article with results for TIP4P/2005 instead given in the supplementary material. In Sec. IV, we then estimate the impact of our findings on the comparison of homogeneous and heterogeneous ice nucleation rates.

As an aside, before proceeding to discuss our main results, we mention that our initial motivation for this study stemmed from recent work by Wang et al.,[41] who developed a new potential that gives broadly similar behavior to the LJ potential but does not suffer, by construction, from ambiguities arising from the choice of truncation scheme. While our preliminary investigations suggested that the approach of Wang et al. could be used to develop workable SPC models of water, we judged their performance insufficiently strong to warrant introducing another set of SPC water models to the

community. We therefore adopt a more pragmatic approach in this article by instead providing results and insights relevant to existing SPC water models that are heavily used by practitioners of molecular simulations.

II. THE MELTING POINT OF ICE I$_h$ FROM FREE ENERGY CALCULATIONS

The central quantity under investigation in this study is the melting point of ice I$_h$ under conditions of vanishing pressure, $p = 0$ bar. To obtain estimates of T_m for TIP4P/ice$^{(r_c)}$ and TIP4P/2005$^{(r_c)}$, we need to establish the chemical potential at $p = 0$ bar for both the ice $[\mu_{ice}(T)]$ and liquid $[\mu_{liq}(T)]$ phases: the point of intersection is T_m. To compute μ_{ice}, we will adopt the Frenkel–Ladd approach,[42] adapted by Vega and co-workers for rigid SPC water models.[43–45] As this approach has been detailed elsewhere, we present a detailed overview of our workflow in the supplementary material and discuss only the most salient aspects of the methodology in the main article.

First, we equilibrate a crystal of ice I$_h$ comprising 768 molecules at a temperature T_i to obtain the average cell parameters. The cell parameters are then fixed to their average values, and the structure is "minimized" by a low temperature simulation at 0.1 K. [We adopt this approach as the standard minimizers in LAMMPS[46] are incompatible with the RATTLE algorithm[47] used to impose the rigid body constraints of the water molecules.] Our reference structure is then this minimized crystal structure with no intermolecular interactions and with the oxygen and hydrogen atoms of each water molecule tethered to their positions by a harmonic potential with spring constants k_O and k_H, respectively. The difference in Helmholtz free energy (per molecule) $\Delta_{r2i}a$ between this reference system and the interacting ice crystal of interest is then calculated by thermodynamic integration[48] at temperature T_i. The rigid body constraints, however, mean that we do not know the free energy of the reference system. We therefore define a "sub-reference" system (with free energy a_{sub} that is calculated analytically) in which only the oxygen atoms of the water molecules are tethered and compute the Helmholtz free energy between the sub-reference and reference systems $\Delta_{s2r}a$ also by thermodynamic integration. The free energy of the ice crystal is then

$$a_{ice} = a_{kin} + a_{sub} + \Delta_{s2r}a + \Delta_{r2i}a - k_B T_i \ln\frac{3}{2} - k_B T_i \ln 2 \quad (10)$$

with $a_{kin} = 3k_B T_i \ln(T_0/T_i)$, where T_0 is a reference temperature (see the supplementary material). We use $T_0 = 272$ K throughout this article. The final two terms, respectively, account for the Pauling entropy arising from proton disorder in ice I$_h$ and the fact that the reference system does not respect the permutational invariance of the two protons in a water molecule.[45] The chemical potential is, in general, obtained from $\beta\mu_{ice} = \beta a_{ice} + \beta p/\bar{\rho}$; as $p = 0$ bar, we simply have $\beta\mu_{ice} = \beta a_{ice}$ ($\beta = 1/k_B T$, where k_B is Boltzmann's constant). We note that there have been extensive studies to understand the effects of finite system size on the calculation of free energies for solids (see Ref. 44 for a detailed discussion). Previous simulation studies suggest that the system size we use (768 molecules) is large enough to obtain a reliable estimate of T_m for ice I$_h$.[49] Moreover, it is likely

that any finite size effects will largely cancel when comparing the two truncation schemes considered in this study.

For the liquid, we equilibrate a system comprising 360 molecules at T_i to obtain an estimate of $\bar{\rho}$. At this density, we then calculate the change in free energy $\Delta_{LJ2w}a$ between the LJ fluid and the SPC water model under investigation using thermodynamic integration. For systems that employ $U^{(r_c \to \infty)}$, we determine the excess free energy of the LJ fluid $a_{LJ,ex}^{(r_c \to \infty)} \approx a_{LJ,ex}^{(\infty)}$ from the equation of state. (For consistency with previous calculations of water's phase diagram,[44] we use the equation of state by Johnson et al.[16]) For systems using $U^{(r_c)}$, we must also compute the free energy difference $\Delta_{tc2cs}a$ between the $U^{(r_c \to \infty)}$ and $U^{(r_c)}$ systems. The free energy of the liquid is then

$$a_{liq}^{(r_c)} = a_{id} + a_{LJ,ex}^{(r_c \to \infty)} + \Delta_{tc2cs}a + \Delta_{LJ2w}a, \qquad (11)$$

where $a_{id} = k_B T_i \ln(\bar{\rho}(T_0/T_i)^3) - k_B T_i$ (see the supplementary material). An analogous expression holds for $a_{liq}^{(r_c \to \infty)}$, except that $\Delta_{tc2cs}a$ is omitted. The chemical potential is simply $\beta\mu_{liq} = \beta a_{liq}$.

Once the chemical potential has been established at T_i, we establish its temperature dependence by integrating the Gibbs–Helmholtz equation,

$$\beta\mu_{ice}(T) = \beta_i\mu_{ice}(T_i) - \int_{T_i}^{T} dt \frac{h_{ice}(t)}{k_B t^2}, \qquad (12)$$

where h_{ice} is the enthalpy per molecule of ice and $\beta_i = 1/k_B T_i$. An analogous expression holds for $\beta\mu_{liq}$.

In Fig. 4(a), we present $\beta\mu_{ice}^{(8.5 \to \infty)}(T)$ and $\beta\mu_{liq}^{(8.5 \to \infty)}(T)$ from which we determine $T_m^{(8.5 \to \infty)} \approx 273.0$ K. This is in good agreement with $T_m^{(8.5 \to \infty)} = 272 \pm 6$ K at $p = 1$ bar obtained by Vega and co-workers.[22,24] The results for TIP4P/ice$^{(8.5)}$ are shown in Fig. 4(b). It is clear that using $U^{(r_c)}$ instead of $U^{(r_c \to \infty)}$ results in an apparent increase in the melting temperature with $T_m^{(8.5)} \approx 276.0$ K. While an increase by ~3 K is modest, it is nonetheless comparable to the difference in melting temperature between D_2O and H_2O.[49,50]

We have not reported an error estimate for either $T_m^{(8.5 \to \infty)}$ or $T_m^{(8.5)}$. Yet, the similarity of the slopes for $\beta\mu_{liq}$ and $\beta\mu_{ice}$ seen in Fig. 4 suggests that even small statistical errors in the chemical potential will result in relatively large changes in the estimate of the melting temperature. Instead of performing a thorough error analysis, in Sec. III, we use a combination of a MF approach and Hamiltonian Gibbs–Duhem integration[51,52] to argue that the difference in T_m reported above reflects a genuine effect of the choice of truncation scheme.

III. A MEAN FIELD ESTIMATE FOR r_c DEPENDENCE OF T_m

We have already seen in Fig. 3(a) that the density of the homogeneous system under isothermal–isobaric conditions is sensitive to the choice of $U^{(r_c)}$ vs $U^{(r_c \to \infty)}$. As indicated by the solid blue line, $\bar{\rho}_m(p)$ is well-described by a quadratic polynomial $r_2 p^2 + r_1 p + r_0$ (see the supplementary material). Using this polynomial approximation in combination with Eqs. (6) and (9), we can predict the
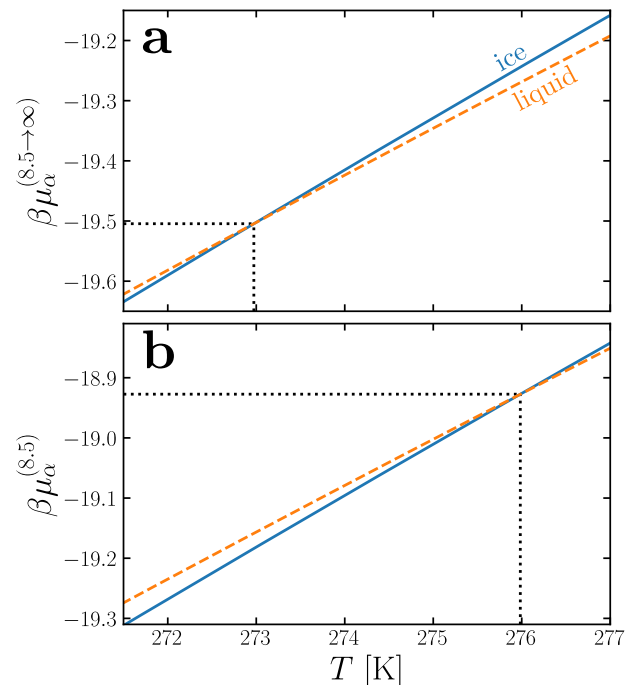

FIG. 4. Locating coexistence: $\beta\mu_\alpha(T)$ at 0 bar with α = "ice" or "liq" for (a) TIP4P/ice$^{(8.5 \to \infty)}$ and (b) TIP4P/ice$^{(8.5)}$. T_m is determined from the point of interception, as indicated by the black dotted lines, with $T_m^{(8.5 \to \infty)} = 273.0$ K and $T_m^{(8.5)} = 276.0$ K.

pressure difference between the $U^{(r_c)}$ and $U^{(r_c \to \infty)}$ systems, as shown by the dashed lines in Fig. 3(a). To validate this MF estimate, we have performed NpT simulations for TIP4P/ice$^{(8.5)}$ at $p = p^{(8.5)}$ predicted by Eq. (9). Excellent agreement between the simulation data and MF estimate is observed. This result is perhaps unsurprising and simply reflects that $r_c = 8.5$ Å $\approx 2.7\sigma$ is sufficiently large to ensure $g_{OO}(r_c) \approx 1$. Nonetheless, it serves as an acute reminder of the effects of the truncation scheme: $\bar{\rho}_m(p = 0)$ for TIP4P/ice$^{(8.5)}$ corresponds to $p \approx -427$ bars for TIP4P/ice$^{(8.5 \to \infty)}$; even for a relatively large cutoff $r_c = 14$ Å $\approx 4.4\sigma$, differences of the order 100 bars persist.

Assuming that $a_{LJ,ex}^{(r_c \to \infty)} \approx a_{LJ,ex}^{(\infty)}$, the Helmholtz free energy per particle for a system with potential energy function $U^{(r_c)}$ can be estimated at a MF level,[16]

$$a_{liq}^{(r_c)} \approx a_{liq}^{(r_c \to \infty)} + \Delta_{MF}a(r_c) \qquad (13)$$

with

$$\Delta_{MF}a(r_c) = -\frac{32\pi\bar{\rho}\epsilon\sigma^3}{9}\left[\left(\frac{\sigma}{r_c}\right)^9 - \frac{3}{2}\left(\frac{\sigma}{r_c}\right)^3\right]. \qquad (14)$$

While MF corrections of the kind given by Eqs. (4), (6), and (14) are strictly appropriate for systems with uniform density, such as homogeneous liquids, they are often employed for crystalline phases

too with evidence to suggest that the obtained results are reasonable.[53] (Note that $\Delta_{MF}a$ approximates the difference in free energy between systems employing $U^{(r_c \to \infty)} \approx U^{(\infty)}$ and $U^{(r_c)}$. In contrast, $\Delta_{MF}U$ approximately accounts for the energy neglected by simply truncating the LJ potential at r_c.) In Figs. 5(a) and 5(b), we show similar analyses as Fig. 3(a) for the liquid and ice phases of TIP4P/ice, respectively, and temperature $T_i = 272$ K, which allow us to predict $\bar{\rho}_m(p = 0)$ for both phases of TIP4P/ice$^{(r_c)}$. Along with Eqs. (13) and (14), this estimate of the density for a given cutoff provides a MF estimate of the chemical potential,

$$\beta\mu^{(MF,r_c)} \approx \beta\mu^{(r_c \to \infty)} + \Delta_{MF}a(r_c). \tag{15}$$

Note that for simplicity, we have ignored any variation of the density with temperature. Results for $\beta\mu^{(MF,8.5)}$ are shown in Fig. 6 from which we deduce a MF estimate for the melting temperature $T_m^{(MF,8.5)} = 275.7$ K; this is in fair agreement with $T_m^{(8.5)} = 276.0$ K obtained from our free energy calculations.

Without performing further simulations, we can use the above procedure to calculate $T_m^{(MF,r_c)}$ for arbitrary r_c, as shown in Fig. 6(b). It can be clearly seen that $T_m^{(MF,r_c)}$ approaches $T_m^{(MF,r_c \to \infty)}$ monotonically and slowly with differences of ~1 K still observed for $r_c = 12$ Å $\approx 3.8\sigma$. Also shown in Fig. 6(b) are estimates of $T_m^{(9.25)}$ = 275.4 K and $T_m^{(10.0)} = 275.1$ K obtained from Hamiltonian

FIG. 6. Predicting the effect of r_c on the melting temperature of TIP4P/ice with MF theory. (a) $\beta\mu_\alpha^{(MF,8.5)}(T)$ at $p = 0$ bar with α = "ice" or "liq," obtained from Eq. (15). $T_m^{(MF,8.5)} = 275.7$ K is determined from the point of interception, as indicated by the black dotted lines. (b) $T_m^{(MF,r_c)}$ is shown by the solid blue line. The orange circle indicates $T_m^{(8.5)}$ obtained from the free energy calculations described in Sec. II, and the orange squares indicate $T_m^{(9.25)}$ and $T_m^{(10.0)}$ obtained from Hamiltonian Gibbs–Duhem integration, starting from $T_m^{(8.5)}$.
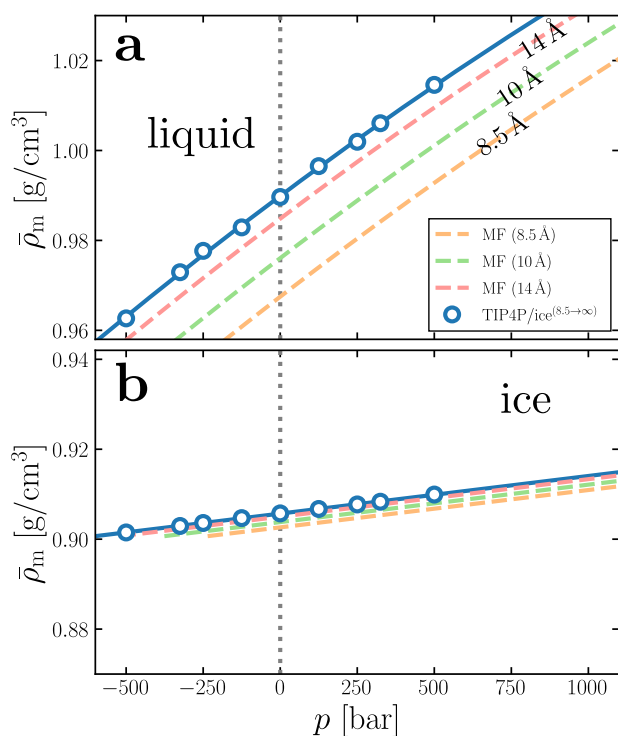

FIG. 5. $\bar{\rho}_m(p)$ at 272 K for (a) liquid water and (b) ice. White-filled circles show results from constant-p simulations of TIP4P/ice$^{(8.5 \to \infty)}$, and the solid blue line indicates a quadratic fit. Dashed lines indicate MF predictions [Eq. (9)] for different r_c, as indicated in the legend, which are used to predict $\bar{\rho}_m(p = 0)$ for a given r_c, i.e., where the dashed lines intersect the vertical gray dotted line.
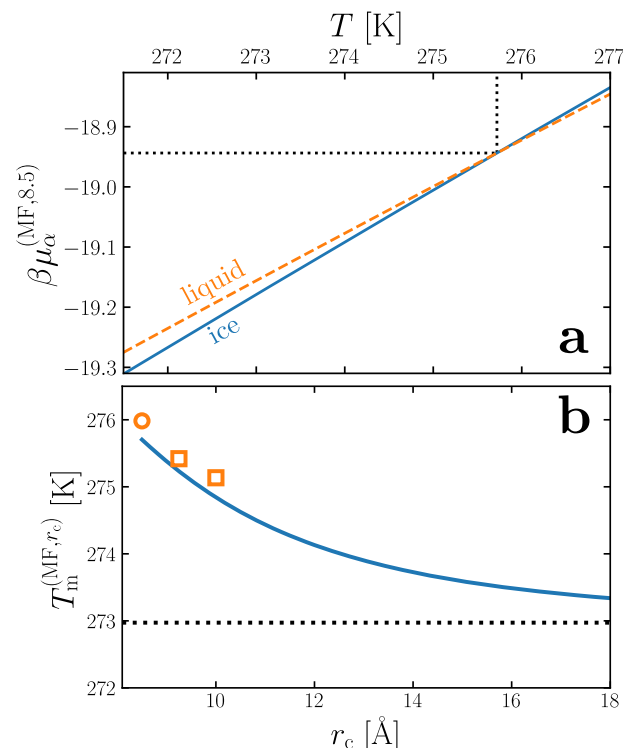
Gibbs–Duhem integration, starting from $T_m^{(8.5)} = 276.0$ K. The observed relative decrease in T_m obtained from Hamiltonian Gibbs–Duhem integration agrees well with that predicted by our MF procedure and provides compelling evidence that reducing r_c results in a systematic increase in the melting temperature. As already mentioned, the increase in T_m with decreasing r_c is modest. We argue that this is a useful observation as obtaining consistent ice nucleation rates among different studies has proven itself to be challenging.[5] Our finding suggests that changes in the degree of supercooling due to differences in r_c are an unlikely source of significant discrepancies in nucleation rates between studies. In Sec. IV, we suggest a way in which effects of the truncation scheme can have a material impact on comparing nucleation rates.

IV. ESTIMATING THE IMPACT ON ICE NUCLEATION RATES

Our results so far indicate that a finite cutoff results in an increase, albeit small, in the melting temperature of SPC models of water. Despite this relatively modest effect on T_m, we nonetheless anticipate that the resulting inconsistencies observed between

homogeneous and inhomogeneous systems may have a significant impact when comparing nucleation rates. In particular, Figs. 3 and 5 suggest that a decrease in r_c is analogous to an increase in pressure (for fixed $\bar{\rho}$). Conversely, for inhomogeneous systems such as those shown in Fig. 2(b), where $U^{(r_c \to \infty)}$ and $U^{(r_c)}$ generate the same dynamics, it is more appropriate to compare to homogeneous nucleation rates computed with $U^{(r_c \to \infty)}$ at $p < 0$ bar rather than at $p = 0$ bar.[54]

To estimate the impact of this effective change in pressure arising from a finite cutoff, we appeal to the recent study by Bianco et al.,[28] where homogeneous nucleation across a broad range of pressures and temperatures for TIP4P/ice$^{(9.0 \to \infty)}$ was investigated and data for $\bar{\rho}(p)$, diffusion coefficient $D(p)$, and size of critical cluster $n_c(p)$ were given. The homogeneous nucleation rate can then be estimated by

$$J(p) = \bar{\rho} f^+ \mathcal{Z} \exp(-\beta \Delta G_c), \tag{16}$$

where $\mathcal{Z} = \sqrt{\beta |\Delta \mu|/(6\pi n_c)}$ and $f^+ = 24 D n_c^{2/3}/(3.8\,\text{Å})^2$. For simplicity, we have assumed $|\Delta \mu| = 0.62$ kJ/mol [see Fig. 3(a) of Ref. 28], independent of pressure; this is justified based on previous studies that find changes in ice/water interfacial tension dominate variations in J with p and is supported by our finding that T_m is only weakly affected by r_c.[27,28] [To gauge the sensitivity of our results to this approximation, the blue shaded region in Fig. 7(b) encompasses predictions obtained with 0.60 kJ/mol $\leq |\Delta \mu| \leq 0.64$ kJ/mol.] In Fig. 7(a), we show $\bar{\rho}(p)$ at $T = 230$ K for TIP4P/ice$^{(r_c \to \infty)}$ from Ref. 28 along with MF estimates for TIP4P/ice$^{(8.5)}$ and TIP4P/ice$^{(11.0)}$. From Fig. 7(a), it can clearly be seen that $\bar{\rho}(p = 0)$ for TIP4P/ice$^{(8.5)}$ and TIP4P/ice$^{(11.0)}$ correspond to $p \approx -400$ bars and $p \approx -200$ bars, respectively. In Fig. 7(b), we plot $\log_{10}[J(p)/J(0)]$ according to Eq. (16) from which we estimate that homogeneous nucleation is faster in TIP4P/ice$^{(8.5)}$ and TIP4P/ice$^{(11.0)}$ by approximately four and two orders of magnitude, respectively.

The implication of the preceding analysis is that enhancement due to heterogeneous nucleation may, in fact, be lower than previously thought. For example, Sosso et al.[55] used a variation of the cut-and-shift potential[56] with $r_c \approx 11$ Å to investigate ice nucleation at 230 K in the presence of kaolinite using FFS and TIP4P/ice. By comparing to the homogeneous nucleation rate obtained by Haji-Akbari and Debenedetti for TIP4P/ice$^{(8.5 \to \infty)}$ with FFS, an enhancement of 20 orders of magnitude was reported; we estimate this result is too high by approximately two orders of magnitude. Similarly, Haji-Akbari and Debenedetti also investigated nucleation in free standing thin films of TIP4P/ice$^{(8.5)}$ water[57] and found an increase of approximately seven orders of magnitude, despite nucleation occurring in bulk-like regions; Fig. 7(b) suggests the nucleation rate of the reference homogeneous system at $p = -400$ bars would also be faster by approximately four orders of magnitude.

This discussion on the impact of the truncation scheme on the nucleation rate is admittedly crude and relies on the analogy that a change in r_c simply amounts to a change in pressure. In practice, it is likely that relevant quantities, e.g., ice–liquid interfacial tension, will differ between TIP4P/ice$^{(r_c \to \infty)}$ at $p < 0$ bar and TIP4P/ice$^{(r_c)}$ at $p = 0$ bar. While the estimates presented above may provide a useful first-order approximation, they await full validation by explicit calculation of nucleation rates using consistent truncation schemes for
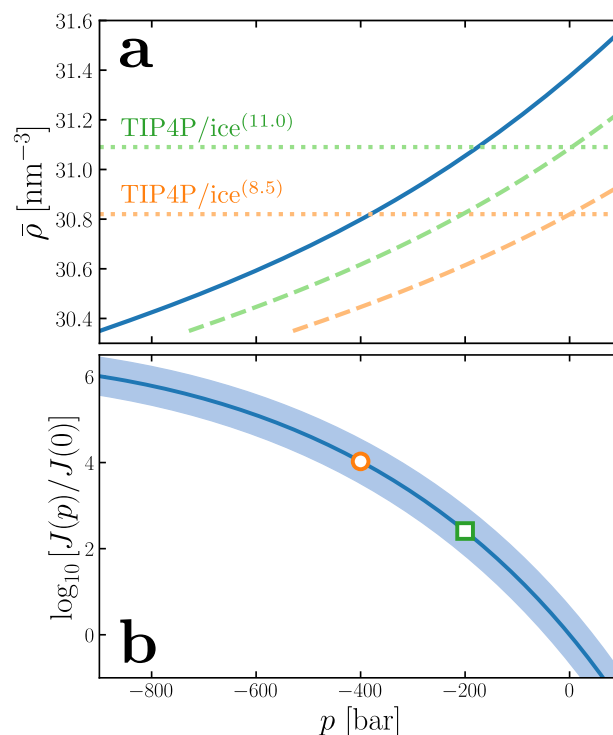

FIG. 7. Estimating the impact on ice nucleation rates. (a) $\bar{\rho}(p)$ for homogeneous liquid water at 230 K. The solid blue line is the result for TIP4P/ice$^{(9.0 \to \infty)}$.[28] Dashed lines indicate MF predictions [Eq. (9)] for TIP4P/ice$^{(8.5)}$ (orange) and TIP4P/ice$^{(11.0)}$ (green); the dotted lines indicate $\bar{\rho}(p = 0)$ for these two cut-and-shift variants. For TIP4P/ice$^{(8.5)}$ and TIP4P/ice$^{(11.0)}$, $\bar{\rho}(p = 0)$, respectively, corresponds to $p \approx -400$ bars and $p \approx -200$ bars for TIP4P/ice$^{(9.0 \to \infty)}$. (b) $\log_{10}[J(p)/J(0)]$ extracted from Ref. 28 with $|\Delta \mu| = 0.62$ kJ/mol. At $p \approx -400$ bars (orange circle) and $p \approx -200$ bars (green square), homogeneous nucleation is approximately four and two orders of magnitude faster, respectively, than at $p = 0$ bar.

homogeneous and inhomogeneous systems. Such calculations are, however, beyond the scope of the present article.

V. SUMMARY AND OUTLOOK

In this article, we have investigated the effect of truncating the Lennard-Jones potential on the melting properties at $p = 0$ bar of two common water models—TIP4P/ice and TIP4P/2005—that are frequently used to study ice nucleation with molecular simulations. Specifically, we have compared results from two truncation schemes: simple truncation at r_c with "tail corrections" and "cut-and-shift" at r_c. We have combined explicit free energy calculations, Hamiltonian Gibbs–Duhem integration, and a simple mean field analysis to show that a finite cutoff results in an increase in the melting temperature. While we have focused on TIP4P/ice and TIP4P/2005, the effects described in this article should be applicable to any reasonable SPC model of water. Moreover, while not an SPC model, we note that the coarse grained mW model[6]—another water model commonly used to investigate ice nucleation—is inherently short-ranged with intermolecular interactions that vanish beyond 4.32 Å. As such, we can

conclude that the mW model will not suffer from the inconsistencies between homogeneous and inhomogeneous systems discussed in this article.

Based on recent work that has investigated homogeneous ice nucleation at negative pressures,[28] we suggest that enhancements due to heterogeneous nucleation calculated by molecular simulations have likely been overestimated by several orders of magnitude. Going forward, those simulating heterogeneous nucleation either need to employ a truncation scheme that effectively samples $U^{(r_c \to \infty)}$,[31–40] or reference data for homogeneous nucleation rates for $U^{(r_c)}$-based SPC models need to be computed explicitly. As a stop-gap solution, one can use the crude but cost-effective estimate for the impact on comparing homogeneous and heterogeneous nucleation rates outlined in this article.

Inconsistencies arising from the choice of truncation scheme are not the only challenges faced when comparing homogeneous and heterogeneous ice nucleation. In particular, we note that Haji-Akbari has shown that conventional FFS approaches can underestimate nucleation rates by failing to account for the "jumpiness" of the order parameter, the severity of which is system dependent.[58] While such subtleties in rate calculations further complicate quantitative comparison of homogeneous and heterogeneous nucleation rates, our work, nonetheless, provides an important contribution toward resolving inconsistencies between homogeneous and inhomogeneous systems. Our results will also facilitate consistent comparison of different studies of heterogeneous ice nucleation.

VI. METHODS

Full details of the methods used are given in the supplementary material. In brief, molecular dynamics simulations were performed with the LAMMPS simulations package.[46] The particle–particle particle-mesh Ewald method was used to account for long-ranged interactions[59] with parameters chosen such that the root mean square error in the forces was a factor 10^5 smaller than the force between two unit charges separated by a distance of 0.1 nm.[60] For simulations of a liquid water slab in contact with its vapor, the electric displacement field along z was set to zero using the implementation given in Refs. 61 and 62; this is formally equivalent to the commonly used slab correction by Yeh and Berkowitz.[63] The geometry of the water molecules was constrained using the RATTLE algorithm.[47] Where appropriate, temperature was maintained with either a Nosé–Hoover chain thermostat[64,65] or Langevin dynamics,[66,67] and pressure was maintained with a Parrinello–Rahman barostat[68] with a damping constant 2 ps. A time step of 2 fs was used throughout. Ice structures were generated using the GenIce software package.[69]

SUPPLEMENTARY MATERIAL

See the supplementary material for a detailed overview of the simulation methods used. The results for the TIP4P/2005 water model are also given.

ACKNOWLEDGMENTS

AUTHOR DECLARATIONS

Conflict of Interest

The authors have no conflicts to disclose.

DATA AVAILABILITY

The data that support the findings of this study are openly available in the data repository at https://doi.org/10.17863/CAM.80092.

REFERENCES

[1] I. Tan, T. Storelvmo, and M. D. Zelinka, Science 352, 224 (2016).

[2] B. Slater, A. Michaelides, C. G. Salzmann, and U. Lohmann, Bull. Am. Meteorol. Soc. 97, 1797 (2016).

[3] M. Bar Dolev, I. Braslavsky, and P. L. Davies, Annu. Rev. Biochem. 85, 515 (2016).

[4] B. J. Murray, D. O'Sullivan, J. D. Atkinson, and M. E. Webb, Chem. Soc. Rev. 41, 6519 (2012).

[5] G. C. Sosso, J. Chen, S. J. Cox, M. Fitzner, P. Pedevilla, A. Zen, and A. Michaelides, Chem. Rev. 116, 7078 (2016).

[6] V. Molinero and E. B. Moore, J. Phys. Chem. B 113, 4008 (2009).

[7] C. Vega and J. L. F. Abascal, Phys. Chem. Chem. Phys. 13, 19663 (2011).

[8] G. A. Cisneros, K. T. Wikfeldt, L. Ojamäe, J. Lu, Y. Xu, H. Torabifard, A. P. Bartók, G. Csányi, V. Molinero, and F. Paesani, Chem. Rev. 116, 7501 (2016).

[9] H. J. C. Berendsen, J. P. M. Postma, W. F. van Gunsteren, and J. Hermans, Intermolecular Forces (D. Reidel Publishing Company, 1981), pp. 331–342.

[10] S. J. Cox, Z. Raza, S. M. Kathmann, B. Slater, and A. Michaelides, Faraday Discuss. 167, 389 (2013).

[11] G. C. Sosso, T. Li, D. Donadio, G. A. Tribello, and A. Michaelides, J. Phys. Chem. Lett. 7, 2350 (2016).

[12] J. E. Lennard-Jones, Proc. Phys. Soc. 43, 461 (1931).

[13] D. Frenkel and B. Smit, Understanding Molecular Simulation, From Algorithms to Applications, 2nd ed. (Academic Press, San Diego, 2002).

[14] M. P. Allen and D. J. Tildesley, Computer Simulation of Liquids, 2nd ed. (Oxford University Press, Oxford, UK, 2017).

[15] B. Smit, J. Chem. Phys. 96, 8639 (1992).

[16] J. K. Johnson, J. A. Zollweg, and K. E. Gubbins, Mol. Phys. 78, 591 (1993).

[17] V. G. Baidakov, G. G. Chernykh, and S. P. Protsenko, Chem. Phys. Lett. 321, 315 (2000).

[18] B. Hafskjold, K. P. Travis, A. B. Hass, M. Hammer, A. Aasen, and Ø. Wilhelmsen, Mol. Phys. 117, 3754 (2019).

[19] A. Ghoufi, P. Malfreyt, and D. J. Tildesley, Chem. Soc. Rev. 45, 1387 (2016).

[20] M. Fitzner, L. Joly, M. Ma, G. C. Sosso, A. Zen, and A. Michaelides, J. Chem. Phys. 147, 121102 (2017).

[21] E. Sanz, C. Vega, J. L. F. Abascal, and L. G. MacDowell, Phys. Rev. Lett. 92, 255701 (2004).

[22] C. Vega, E. Sanz, and J. L. F. Abascal, J. Chem. Phys. 122, 114507 (2005).

[23] J. L. F. Abascal and C. Vega, J. Chem. Phys. 123, 234505 (2005).

[24] J. L. F. Abascal, E. Sanz, R. García Fernández, and C. Vega, J. Chem. Phys. 122, 234511 (2005).

[25] J. R. Espinosa, E. Sanz, C. Valeriani, and C. Vega, J. Chem. Phys. 141, 18C529 (2014).

[26] A. Haji-Akbari and P. G. Debenedetti, Proc. Natl. Acad. Sci. U. S. A. 112, 10582 (2015).

[27] J. R. Espinosa, A. Zaragoza, P. Rosales-Pelaez, C. Navarro, C. Valeriani, C. Vega, and E. Sanz, Phys. Rev. Lett. 117, 135702 (2016).

[28] V. Bianco, P. M. de Hijes, C. P. Lamas, E. Sanz, and C. Vega, Phys. Rev. Lett. **126**, 015704 (2021).

[29] Figure 3(b) in fact shows the number density profile converted to mass density. While the two profiles will differ slightly near the interface, they are the same in the bulk region of interest in this study.

[30] J. Rowlinson and B. Widom, *Molecular Theory of Capillarity*, Dover Books on Chemistry (Dover Publications, 2002).

[31] P. J. in't Veld, A. E. Ismail, and G. S. Grest, J. Chem. Phys. **127**, 144711 (2007).

[32] J. Alejandre and G. A. Chapela, J. Chem. Phys. **132**, 014701 (2010).

[33] J. López-lemus and J. Alejandre, Mol. Phys. **100**, 2983 (2002).

[34] J. López-lemus and J. Alejandre, Mol. Phys. **101**, 743 (2003).

[35] J. M. Míguez, M. M. Piñeiro, and F. J. Blas, J. Chem. Phys. **138**, 034707 (2013).

[36] J. Janeček, J. Phys. Chem. B **110**, 6264 (2006).

[37] E. Salomons and M. Mareschal, J. Phys.: Condens. Matter **3**, 9215 (1991).

[38] M. Guo, D.-Y. Peng, and B. C.-Y. Lu, Fluid Phase Equilib. **130**, 19 (1997).

[39] M. Guo and B. C.-Y. Lu, J. Chem. Phys. **106**, 3688 (1997).

[40] R. de Gregorio, J. Benet, N. A. Katcho, F. J. Blas, and L. G. MacDowell, J. Chem. Phys. **136**, 104703 (2012).

[41] X. Wang, S. Ramírez-Hinestrosa, J. Dobnikar, and D. Frenkel, Phys. Chem. Chem. Phys. **22**, 10624 (2020).

[42] D. Frenkel and A. J. C. Ladd, J. Chem. Phys. **81**, 3188 (1984).

[43] E. G. Noya, M. M. Conde, and C. Vega, J. Chem. Phys. **129**, 104704 (2008).

[44] C. Vega, E. Sanz, J. L. F. Abascal, and E. G. Noya, J. Phys.: Condens. Matter **20**, 153101 (2008).

[45] J. L. Aragones, E. G. Noya, C. Valeriani, and C. Vega, J. Chem. Phys. **139**, 034104 (2013).

[46] S. Plimpton, J. Comput. Phys. **117**, 1 (1995).

[47] H. C. Andersen, J. Comput. Phys. **52**, 24 (1983).

[48] J. G. Kirkwood, J. Chem. Phys. **3**, 300 (1935).

[49] A. Reinhardt and B. Cheng, Nat. Commun. **12**, 588 (2021).

[50] E. Bartholomè and K. Clnsins, Z. Phys. Chem. **28B**, 167 (1935).

[51] R. Agrawal and D. A. Kofke, Phys. Rev. Lett. **74**, 122 (1995).

[52] R. Agrawal and D. A. Kofke, Mol. Phys. **85**, 23 (1995).

[53] K. M. Jablonka, D. Ongari, and B. Smit, J. Chem. Theory Comput. **15**, 5635 (2019).

[54] It would, of course, be most appropriate to compare to homogeneous nucleation rates obtained with $U^{(r_c)}$ at p = 0 bar. Such reference data are, however, scarce.

[55] G. C. Sosso, G. A. Tribello, A. Zen, P. Pedevilla, and A. Michaelides, J. Chem. Phys. **145**, 211927 (2016).

[56] To be concrete, Sosso *et al.*[55] considered LJ interactions up to 10 Å, where a switching function was used to bring them to zero at 12 Å. Without validation, we simply approximate this by TIP4P/ice$^{(11.0)}$.

[57] A. Haji-Akbari and P. G. Debenedetti, Proc. Natl. Acad. Sci. U. S. A. **114**, 3316 (2017).

[58] A. Haji-Akbari, J. Chem. Phys. **149**, 072303 (2018).

[59] R. W. Hockney and J. W. Eastwood, *Computer Simulation Using Particles* (CRC Press, 1988).

[60] J. Kolafa and J. W. Perram, Mol. Simul. **9**, 351 (1992).

[61] S. J. Cox and M. Sprik, J. Chem. Phys. **151**, 064506 (2019).

[62] T. Sayer and S. J. Cox, Phys. Chem. Chem. Phys. **21**, 14546 (2019).

[63] I.-C. Yeh and M. L. Berkowitz, J. Chem. Phys. **111**, 3155 (1999).

[64] W. Shinoda, M. Shiga, and M. Mikami, Phys. Rev. B **69**, 134103 (2004).

[65] M. E. Tuckerman, J. Alejandre, R. López-Rendón, A. L. Jochim, and G. J. Martyna, J. Phys. A: Math. Gen. **39**, 5629 (2006).

[66] B. Dünweg and W. Paul, Int. J. Mod. Phys. C **02**, 817 (1991).

[67] T. Schneider and E. Stoll, Phys. Rev. B **17**, 1302 (1978).

[68] M. Parrinello and A. Rahman, J. Appl. Phys. **52**, 7182 (1981).

[69] M. Matsumoto, T. Yagasaki, and H. Tanaka, J. Comput. Chem. **39**, 61 (2018).